

## Coexistence of metallic and nonmetallic charge transport in $\text{PrBa}_2\text{Cu}_3\text{O}_7$

Mark Lee

*Department of Physics, University of Virginia, Charlottesville, Virginia 22903*

Y. Suzuki\* and T. H. Geballe

*Department of Applied Physics, Stanford University, Stanford, California 94305*

(Received 15 December 1994)

Magnetotransport measurements on highly oriented thin films of  $\text{PrBa}_2\text{Cu}_3\text{O}_7$  demonstrate a unique coexistence of nonmetallic hopping conduction with metallic Boltzmann transport. At high temperature ( $T > 10$  K) hopping transport dominates, but when the inelastic conduction freezes out at low temperature, metallic behavior can be distinguished. The hopping conduction is assigned to the  $\text{CuO}_2$  planes, while the Boltzmann transport arises from the  $\text{CuO}$  chain structure, in agreement with recent electronic-structure calculations.

Alone among the family of perovskite rare-earth barium cuprates  $\text{RBa}_2\text{Cu}_3\text{O}_7$ ,  $\text{PrBa}_2\text{Cu}_3\text{O}_7$  (PrBCO) lacks many metallic properties common to its isostructural superconductor relatives. For this reason, PrBCO has been widely investigated in the hope that discerning the reason for its singular nonmetallic behavior will clarify the properties of the high- $T_c$  superconductors.<sup>1</sup> There has also been great interest in PrBCO as an epitaxial barrier in Josephson junctions. Most studies of PrBCO report a divergent low-temperature resistivity  $\rho(T)$  that is often, though not always, in the form of variable-range hopping.<sup>2</sup> Hopping is observed in many semiconductors doped below the critical density of a metal-insulator transition. However, a collection of recent experiments studying PrBCO transport in either submicron structures or more ordered samples have cast doubt on whether PrBCO is truly a nonmetal. Hashimoto *et al.*<sup>3</sup> discovered that Josephson coupling between superconducting  $\text{YBa}_2\text{Cu}_3\text{O}_7$  (YBCO) electrodes can occur across  $\geq 0.1 \mu\text{m}$  of PrBCO, a length scale normally associated with dirty metal weak links. Kabasawa *et al.*<sup>4</sup> found that the  $\rho(T \rightarrow 0)$  divergence cuts off at length scales of  $\approx 0.2 \mu\text{m}$ . Hoffman *et al.*<sup>5</sup> observed by positron annihilation a metallic Fermi-surface sheet assigned to the  $\text{CuO}$  chains. Takenaka *et al.*<sup>6</sup> reported that the integrated  $b$ -axis ( $\text{CuO}$  chain direction) optical conductivity in an untwinned PrBCO crystal was of the same order as in YBCO at 300 K. These data led Fehrenbacher and Rice<sup>7</sup> to propose that a  $\text{Pr } 4f\text{-O } 2p_\pi$  hybridization removes holes from the  $\text{CuO}_2$  planes, while leaving the chains unperturbed. Recent experiments on oxygen- and cobalt-doped PrBCO by Suzuki *et al.*<sup>8</sup> showed strong evidence that hopping transport occurs on the planes, and that the chain conductivity was unusually large.

All the above experiments hint at a coexistence between metallic and nonmetallic conduction that would make PrBCO unique among all materials studied in metal-insulator physics. The definitive test of metallic behavior comes from the low-temperature charge transport behavior. In this paper we present data on the resistivity, magnetoresistance (MR), and Hall effect which,

when considered together, demonstrate that charge transport along the chain direction in PrBCO films possesses distinctly *metallic* characteristic at low temperature in samples where the chains have macroscopic continuity. Such properties are not as evident in heavily twinned samples where the  $b$  axis has no macroscopic continuity, implying that the metallic conduction is associated with holes on the  $\text{CuO}$  chains, in agreement with Refs. 5–8. These results also account for the anomalous Josephson coupling observed in Ref. 3.

PrBCO films 150 to 350 nm thick were deposited by  $90^\circ$  off-axis sputtering.<sup>9</sup> As depicted in Fig. 1, two types of PrBCO films were studied. The first were “nonaligned” films, where the  $c$  axis (normal to the  $\text{CuO}_2$  planes) is perpendicular to the substrate. We measured seven nonaligned films grown on  $\text{LaAlO}_3$  and  $\text{MgO}$  substrates. In these films, twinned grain boundaries interrupt the continuity of the  $b$  axis. Transmission electron microscopy (TEM) showed twin-free domain sizes ranging from 0.1 to  $0.5 \mu\text{m}$ , limiting the continuity of the chain structure to these distances. The second type of samples were “in-plane aligned” films, where the  $a$  axis is normal to the substrate, while the  $b$  and  $c$  axes have a well-defined macroscopic in-plane alignment over the sample dimensions.<sup>10,11</sup> Details of the deposition and characterization of in-plane aligned films are given in Ref. 10. We measured four such films. For three of these

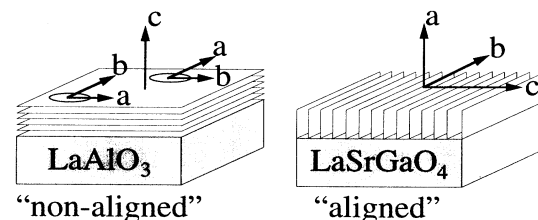


FIG. 1. Picture of the orientations of nonaligned and aligned films. The  $b$  axis denotes the  $\text{CuO}$  chain direction, the  $a$  axis is the  $\text{CuO}_2$  plane direction orthogonal to  $b$ , and the  $c$  axis is perpendicular to both planes and chains.

films, two grown on  $\text{LaSrGaO}_4$  and one on  $\text{NdGaO}_3$ , x-ray diffraction ratios of the  $a$ -axis normal reflection to all other reflections was  $\geq 99:1$ , and the in-plane  $c$ -axis reflections comprised  $>95\%$  of the total in-plane reflection peak intensities. These will be referred to as “99%-aligned” samples. For the other in-plane aligned film on  $\text{LaSrGaO}_4$ , the ratio of x-ray intensities of the  $a$ -axis normal peak to  $b$ -axis normal peak was 65:35. This will be referred to as the “65%-aligned” sample. TEM showed that the defect structures in the aligned films were antiphase and  $90^\circ$  tilt boundaries. Ohmic contacts spaced 1 mm apart were made with silver. The current  $\mathbf{J}$  was normal to the  $c$  axis in all samples. Resistivity values were calculated from the measured resistances using the nominal contact geometry and film thicknesses.

Figure 2 shows  $\rho(T)$  from 120 to 1 K for a nonaligned sample, the 65%-aligned sample along the nominal  $b$  axis, and one of the 99%-aligned samples along the  $b$  axis. All other nonaligned and 99%-aligned samples displayed similar behavior. In the main figure,  $\rho(T)$  is plotted on a log scale vs  $T^{-1/4}$  to emphasize the hopping transport<sup>12</sup> both in the nonaligned sample and in  $T > 10$  K range for the 65%-aligned sample. Going from nonaligned to more aligned samples, the resistivity becomes strikingly less temperature dependent. The nonaligned sample  $\rho(T)$  increases almost five decades in a manner consistent with hopping. Below 5 K  $\rho(T)$  increases slightly faster than  $T^{-1/4}$  behavior. The 65%-aligned sample displays two distinct regimes: a higher-temperature hopping transport similar to the nonaligned sample, crossing over below 7 K to a weakly temperature-dependent resistivity. For the 99%-aligned sample,  $\rho(T)$  increases less than one decade through the temperature range but cannot be fitted to any common type of hopping behavior. The low-temperature resistivity in this sample is almost constant. Unlike the 65%-aligned sample, the low-temperature behavior of the 99%-aligned samples evolves smoothly from higher temperatures without a distinct crossover.

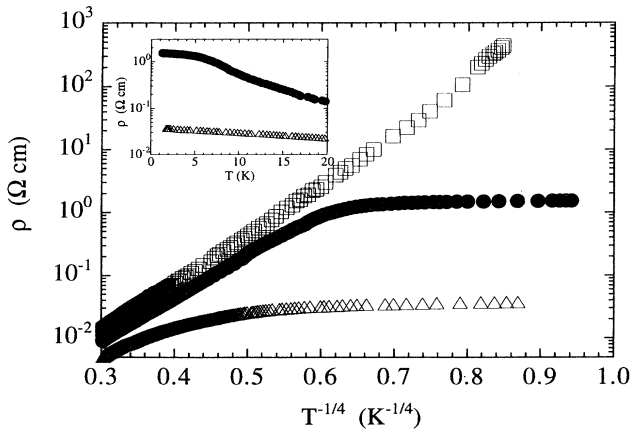


FIG. 2. Resistivities vs  $T^{-1/4}$  for a nonaligned sample (open squares) in the  $a, b$  plane, a 65% in-plane aligned sample (black circles) along the nominal  $b$  axis, and a 99%-aligned sample (open triangles) along the  $b$  axis. Inset:  $\rho$  plot against linear  $T$  for the aligned samples (same symbols as in the main figure).

For all the in-plane aligned samples, plotting  $\rho$  against linear  $T$  (Fig. 2 inset) and extrapolating smoothly to  $T=0$  yielded a finite value,  $\approx 0.03 \Omega \text{ cm}$  for the 99%-aligned samples and  $\approx 1.5 \Omega \text{ cm}$  for the 65%-aligned sample. The data for the 65%-aligned sample fit reasonably well to a parallel resistor model consisting of one hopping path and one constant resistivity path, but the data for the 99%-aligned samples do not. The value of  $\rho(T \rightarrow 0)$  for the 65%-aligned sample is seemingly too high to be consistent with ordinary metallic conduction. The data from the 99%-aligned sample are more representative of homogeneous  $b$ -axis transport and suggest that the low-temperature resistivity of the 65%-aligned sample results from filamentary metallic links short circuiting the higher-resistance hopping channels. Consequently, the nominal sample geometry is larger than the actual (unknown) conduction cross section and hence overstates the true resistivity.

While a finite  $\rho(T \rightarrow 0)$  value technically defines metallic transport, supporting evidence for such behavior can be found by examining the magnetoresistance (MR). The functional descriptions that follow apply to all the nonaligned and in-plane aligned samples measured, except with different magnitudes, as noted below. Figure 3 shows both transverse ( $\mathbf{H} \parallel c; \mathbf{J} \parallel b$ ) and longitudinal ( $\mathbf{H} \parallel \mathbf{J} \parallel b$ ) MR data on both a nonaligned and a 99%-aligned sample. Above  $\sim 14$  K, both types of samples show a negative transverse MR that saturates at  $\sim 0.4\%$  to  $\sim 0.6\%$  above 4 T. When the temperature is lowered, the MR qualitatively changes character. Below 5 K the transverse MR is strictly positive and  $\propto H^2$  over field scales of several teslas, while the longitudinal MR at the same temperature and fields is negligibly small. The negative-to-positive evolution of the transverse MR was evident for all samples. Figure 4 shows the trend by plotting the transverse MR at 3 T vs temperature for the 65%-aligned sample. A saturated negative transverse MR first becomes apparent around 20 K, bottoms out between 8 and 12 K, and then becomes positive and  $\propto H^2$

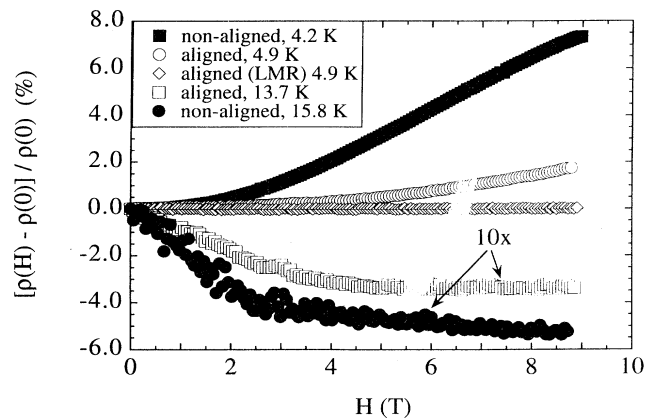


FIG. 3. The normalized magnetoresistance as a function of magnetic field for a 99%-aligned sample and a nonaligned sample. The 13.7 and 15.8 K data are expanded by a factor of 10 for clarity. Data are for the transverse geometry except the white diamonds, which are for the longitudinal (LMR) geometry.

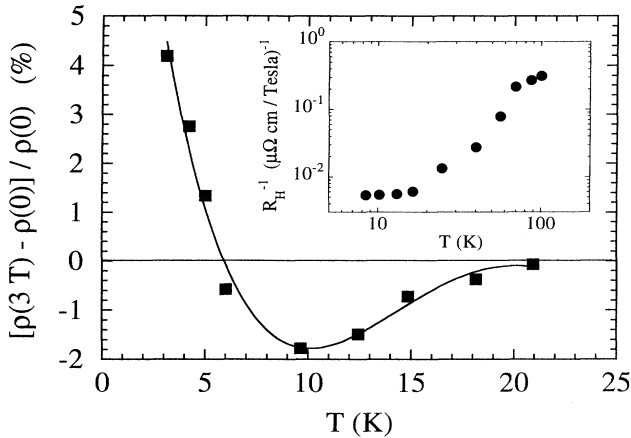


FIG. 4. The temperature dependence of the transverse MR at 3 T for the 65%-aligned sample. The curve is a guide to the eye. Inset: The temperature dependence of the inverse Hall coefficient on nonaligned sample.

at lower temperature. Larger magnitude changes were systematically observed in the nonaligned samples, which reached  $\sim +2\%$  (at 4.2 K) at 3 T, compared to  $+1.4\%$  for the 65%-aligned sample (see Fig. 4) and  $\sim +0.5\%$  for the 99%-aligned samples at 3 T between 4 and 5 K. We note that a low-temperature, high-field MR  $\propto H^2$  in PrBCO was reported by Iwasaki *et al.*<sup>13</sup>

The higher-temperature negative MR is consistent with hopping conduction.<sup>14</sup> We cannot yet distinguish between forward scattering<sup>15</sup> and increasing localization length<sup>16</sup> mechanisms. Either way, it indicates that even in the 99%-aligned samples, some component of the current at higher temperature is carried by hopping. However, the change in sign and form of the MR at lower temperature is uncharacteristic of hopping conduction. Because MR in hopping systems arises from competition between wave-function trajectory effects and material-dependent interactions, such as spin-orbit coupling, different hopping systems display a large variety of field dependencies with either sign.<sup>17</sup> For instance, Ochiai<sup>18</sup> observed a large ( $+50\%$  at 3.9 K) MR  $\propto H^2$  in barely insulating Si:Sb. Giant ( $\geq +1000\%$ ) quasiexponential MR's have been measured by several groups and attributed to wave-function shrinkage.<sup>19</sup> However, these experiments show that decreasing temperature only increases the MR magnitude and does not reverse the sign or qualitatively change the functional form. In this respect the temperature dependence of the data in Figs. 3 and 4 strongly indicates that the positive MR we observed is unrelated to hopping.

The positive transverse MR may arise either from semiclassical orbital effects<sup>20</sup> associated with Boltzmann transport, or from Kondo-like magnetic scattering.<sup>21</sup> These mechanisms are distinguished by the fact that the longitudinal MR is negligibly small at the same temperatures at which the transverse MR is significantly large. Longitudinal MR arises only from isotropic scattering, since there is no Lorentz force. The zero longitudinal MR thus provides a clear indication that the observed positive transverse MR is an orbital rather than spin

effect. The magnitude ( $\sim$  few%) and square-law form of the positive transverse MR are typical of "low" field (in the sense  $\omega_c \tau < 1$ ) Boltzmann transport in an anisotropic disordered metal.

In this context the observed positive MR in nonaligned samples with divergent  $\rho(T \rightarrow 0)$  may be surprising. However, this can be reconciled by noting that the orbital MR is sensitive to field-induced changes in the trajectory of the charge wave function. The orbital  $+H^2$  correction to the resistivity can be viewed as arising from Lorentz-force bending of the wave-function orbits with a bend radius of roughly the magnetic length  $l_H = (\hbar c / eH)^{1/2}$ . In all cases, including the nonaligned samples, the orbital MR is measurable only over field scales of teslas, corresponding to  $l_H$  much less than the typical twin-free domain size ( $\leq 0.5 \mu\text{m}$  as measured by TEM). Consequently, the observed MR in the nonaligned samples probes transport in regions free of twinning disorder. The positive MR  $\propto H^2$  in nonaligned samples can therefore be taken as a signature of metallic orbital effects occurring over distances where the chain conduction is continuous. This model is supported by the direct observation in Ref. 4 of metallic resistivity only when a channel length fell below  $\sim 0.2 \mu\text{m}$  in nonaligned PrBCO films. The MR magnitude can be greater in nonaligned samples compared to the aligned samples, for both positive and negative MR, simply because the field-induced orbits in aligned samples are forced to partially traverse the high resistivity  $c$  direction. The scattering lifetime  $\tau_{ab}$  for  $a, b$ -plane orbits is always larger than  $\tau_{bc}$  for  $b, c$ -plane orbits, so that  $\omega_c \tau_{ab} > \omega_c \tau_{bc}$  at any given field.

Final evidence for low-temperature metallic behavior in PrBCO comes from the temperature dependence of the inverse Hall coefficient,  $R_H^{-1}$ . Figure 4 (inset) shows  $R_H^{-1}$  vs  $T$  taken on a nonaligned sample in fields parallel to the  $c$  axis. Hall data on aligned samples are unreliable due to large potential drops across the in-plane  $c$  axis on these films. The Hall resistivity  $\rho_{xy} = R_H H$  was linear with magnetic field up to at least 5 T at all temperatures.  $R_H^{-1}$  falls by over one decade as temperature decreases from 100 to 8 K, but saturates at a nonzero value at low temperature. While it is misleading to derive a carrier density from the Hall data in an anisotropic multiband material, the strong temperature dependence of  $R_H^{-1}$  at high temperature implies that some, though not all, carriers may arise from some form of thermal activation. At low temperature, the constant Hall coefficient is certainly consistent with metallic conduction, though by itself it cannot exclude the possibility of nonmetallic transport.

Each individual part of the data discussed, i.e., the saturation of  $\rho(T \rightarrow 0)$  in the aligned samples, the low-temperature crossover from negative to positive MR over fields of several teslas, and the low-temperature saturation of the Hall coefficient, may be open to different, unrelated explanations. We believe that these results in combination permit a simple and consistent interpretation as evidence of a metallic conduction mechanism taking over from a nonmetallic one at sufficiently low temperature. This is observable in the macroscopic zero-field resistivity only for samples with sufficient alignment of CuO chains, but may appear in twinned samples when

the field deflection radius becomes comparable to the twin-free domain size.

The coexistence of hopping conduction on the  $\text{CuO}_2$  planes with a metallic  $\text{CuO}$  chain structure is at least qualitatively consistent with the model of Fehrenbacher and Rice.<sup>7</sup> Taking the ground state of the  $\text{CuO}_2$  plane to consist of holes hybridized into  $\text{Pr}^{\text{III}} + \text{Pr}^{\text{IV}}$ , as proposed by these authors, the Hall and  $\rho(T)$  data on nonaligned samples show that this ground state is fully localized. However, macroscopic nonmetallic behavior now appears, as suggested in Ref. 7, to be an extrinsic property of PrBCO that is highly sensitive to the degree of structural disorder.

Low-temperature metallic chain conduction can account for both the existence and the temperature dependence of the long-ranged Josephson coupling reported in Ref. 3 and more recently by others.<sup>22</sup> They found that  $a$ -axis YBCO-PrBCO-YBCO junctions can sustain a Josephson effect through  $\geq 0.1 \mu\text{m}$  of PrBCO at 4.2 K, but that the junction supercurrent vanished around 25 K, though the YBCO was still superconducting. Josephson length scales  $\geq 0.01 \mu\text{m}$  normally arise from Cooper pair diffusion through a metallic weak link, rather than from quantum tunneling. The chain paths provide a natural metallic coupling path, so long as the chains are continuous across the junction. This was suggested as the origin of long vortex coupling lengths observed in Ref. 8. The grain sizes in nonaligned PrBCO films set an upper bound of  $\sim 0.5 \mu\text{m}$  on the chain continuity distance. Further-

more, above a temperature that is typically less than the  $T_c$  of YBCO, inelastic hopping conduction becomes the favored transport mechanism in PrBCO. Such hopping does not preserve phase coherence and is incompatible with Josephson coupling. Therefore, the supercurrent through "thick" ( $\sim 0.1 \mu\text{m}$ ) PrBCO barriers should vanish well below the  $T_c$  of YBCO, as has been observed in Refs. 3 and 22.

In summary, we have measured three aspects of low-temperature charge transport in both nonaligned and in-plane aligned PrBCO thin films. These show that at high temperature the conduction is primarily inelastic. However, the combination of a finite  $\rho(T \rightarrow 0)$  in the aligned samples, a positive transverse  $\text{MR} \propto H^2$  at high fields, and a temperature-independent Hall coefficient can all be explained by one premise: the presence of metallic chains. In the aligned samples, the metallic nature exists over macroscopic length scales. In nonaligned samples, there is evidence of metallic behavior only at the submicron level. These findings explain the anomalous range and temperature dependence of Josephson junctions using PrBCO as a weak link.

We thank N. S. Wingreen and Y. Meir for thought-provoking discussions. Work at U.Va. was supported in part by NSF Grant No. DMR-9316803. Work at Stanford was supported by the AFOSR and EPRI. Y.S. acknowledges support from NSF.

\*Present address: AT&T Bell Laboratories, Murray Hill, NJ 07979.

<sup>1</sup>H. B. Radousky, *J. Mater. Res.* **7**, 1917 (1992).

<sup>2</sup>B. Fisher *et al.*, *Physica C* **176**, 75 (1991).

<sup>3</sup>T. Hashimoto *et al.*, *Appl. Phys. Lett.* **60**, 1756 (1992).

<sup>4</sup>U. Kabasawa *et al.*, *Phys. Rev. Lett.* **70**, 1700 (1993).

<sup>5</sup>L. Hoffman *et al.*, *Phys. Rev. Lett.* **71**, 4047 (1993).

<sup>6</sup>K. Takenaka *et al.*, *Phys. Rev. B* **46**, 5833 (1992).

<sup>7</sup>R. Fehrenbacher and T. M. Rice, *Phys. Rev. Lett.* **70**, 3471 (1993).

<sup>8</sup>Y. Suzuki *et al.*, *Phys. Rev. Lett.* **73**, 328 (1994).

<sup>9</sup>C. B. Eom *et al.*, *Appl. Phys. Lett.* **55**, 595 (1989).

<sup>10</sup>Y. Suzuki *et al.*, *Phys. Rev. B* **48**, 10 642 (1993).

<sup>11</sup>K. H. Young and J. Z. Sun, *Appl. Phys. Lett.* **59**, 2448 (1991); S. Hontsu *et al.*, *Appl. Phys. Lett.* **61**, 1134 (1992); M. Mukaida and S. Miyazawa, *ibid.* **63**, 999 (1993).

<sup>12</sup>Reference 4 favors a two-dimensional hopping exponent  $\nu = \frac{1}{3}$ , while Ref. 8 uses the three-dimensional form  $\nu = \frac{1}{4}$ . The exponent can be determined without prejudice from the slope of  $\log_{10}[\partial \log_e(\rho) / \partial \log_e(1/T)]$  vs  $\log_{10}(T)$ , as derived by A. G. Zabrodskii and K. N. Zinov'eva, *Zh. Eksp. Teor. Fiz.* **86**, 727 (1984) [*Sov. Phys. JETP* **59**, 425 (1984)]. Applying this to the nonaligned sample data of Fig. 2 between 10

and 120 K yields an exponent of 0.27. The more three-dimensional nature of the hopping may arise from scattering between the closely spaced  $\text{CuO}_2$  planes.

<sup>13</sup>H. Iwasaki *et al.*, *Physica C* **204**, 406 (1993).

<sup>14</sup>Z. Ovadyahu, *Phys. Rev. B* **33**, 6552 (1986); O. Faran and Z. Ovadyahu, *ibid.* **38**, 5457 (1988); F. Tremblay *et al.*, *ibid.* **40**, 10 052 (1989).

<sup>15</sup>V. L. Nguen, B. Z. Spivak, and B. I. Shklovskii, *Zh. Eksp. Teor. Fiz.* **89**, 1770 (1985) [*Sov. Phys. JETP* **62**, 1021 (1985)]; Y. Meir and O. Entin-Wohlman, *Phys. Rev. Lett.* **70**, 1988 (1993).

<sup>16</sup>J.-L. Pichard *et al.*, *Phys. Rev. Lett.* **65**, 1812 (1990).

<sup>17</sup>*Hopping and Related Phenomena*, edited by H. Fritzsche and M. Pollak (World Scientific, New Jersey, 1990).

<sup>18</sup>Y. Ochiai, as reported in Ref. 17, p. 25.

<sup>19</sup>B. I. Shklovskii and A. L. Efros, *Electronic Properties of Doped Semiconductors* (Springer-Verlag, New York, 1984).

<sup>20</sup>A. B. Pippard, *Magnetoresistance in Metals* (Cambridge Univ. Press, Cambridge, 1989).

<sup>21</sup>V. Zlatic, *J. Phys. F* **11**, 2147 (1981).

<sup>22</sup>T. Umezawa *et al.*, *Appl. Phys. Lett.* **63**, 3221 (1993); H. Sato, H. Akoh, and S. Takada, *ibid.* **64**, 1286 (1994).

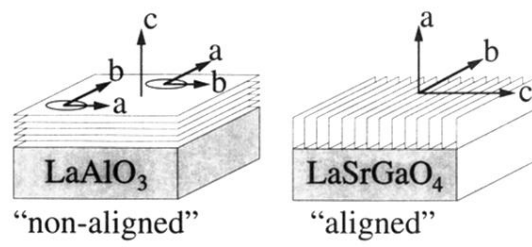


FIG. 1. Picture of the orientations of nonaligned and aligned films. The  $b$  axis denotes the CuO chain direction, the  $a$  axis is the  $\text{CuO}_2$  plane direction orthogonal to  $b$ , and the  $c$  axis is perpendicular to both planes and chains.